aerospace

MDPI

Article

Turbulence Effects on Modified State Observer-Based Adaptive Control: Black Kite Micro Aerial Vehicle

Venkatasubramani S. R. Pappu [1,*], James E. Steck [1,†] and Guruganesh Ramamurthi [2,†]

[1] Department of Aerospace Engineering, Wichita State University, Wichita, KS 67260, USA; james.steck@wichita.edu

[2] CSIR–National Aerospace Laboratories, Bangalore 560017, India; rguruganesh@nal.res.in

* Correspondence: vxsubbareddiarpappu@wichita.edu; Tel.: +1-316-558-2152

† These authors contributed equally to this work.

Academic Editor: Michael Wing

Received: 1 November 2015; Accepted: 26 January 2016; Published: 5 February 2016

Abstract: This paper presents the implementation of a modified state observer-based adaptive dynamic inverse controller for the Black Kite micro aerial vehicle. The pitch and velocity adaptations are computed by the modified state observer in the presence of turbulence to simulate atmospheric conditions. This state observer uses the estimation error to generate the adaptations and, hence, is more robust than model reference adaptive controllers which use modeling or tracking error. In prior work, a traditional proportional-integral-derivative control law was tested in simulation for its adaptive capability in the longitudinal dynamics of the Black Kite micro aerial vehicle. This controller tracks the altitude and velocity commands during normal conditions, but fails in the presence of both parameter uncertainties and system failures. The modified state observer-based adaptations, along with the proportional-integral-derivative controller enables tracking despite these conditions. To simulate flight of the micro aerial vehicle with turbulence, a Dryden turbulence model is included. The turbulence levels used are based on the absolute load factor experienced by the aircraft. The length scale was set to 2.0 meters with a turbulence intensity of 5.0 m/s that generates a moderate turbulence. Simulation results for various flight conditions show that the modified state observer-based adaptations were able to adapt to the uncertainties and the controller tracks the commanded altitude and velocity. The summary of results for all of the simulated test cases and the response plots of various states for typical flight cases are presented.

Keywords: modified state observer; adaptive control; micro aerial vehicle

1. Introduction

Micro aerial vehicles (MAV) have recently gathered much attention for use in both civil and military applications. Research is being carried out in developing a robust and safe micro aerial vehicles in various laboratories all over the world. Effort is also made to develop a feasible flight certification of the vehicle.

In order to build a robust vehicle which can be flown in uncertain environments and also by less-skilled pilots, adaptive control systems have been developed for general aviation aircraft at Wichita State University. The work has been based on the neural network based model reference adaptive controller (MRAC) work at NASA, by J.E. Steck and others [1–3]. The published research work were referred to aid in the development of the flight control system for the Black Kite MAV model. Arning *et al.* [4] shows an integrated autopilot design for DO-MAV using Micro Electro Mechanical System (MEMS) sensors. They presented an optimized flight control law design for roll control by varying the aircraft configuration and control parameters. Jordan *et al.* [5] described the

development of a 5.5% scaled unmanned aerial vehicle (UAV) testbed named AirSTAR, designed to investigate the dynamics and control of a large transport airplane in the upset conditions in the flight envelope. The paper gives details about the overall program structure including the scaled model design, ground station functionalities, and flight test capability. Knoebel *et al.* [6] developed a MRAC-based adaptive control algorithm for pitch and roll attitude holds of an MAV. Flight tests were conducted for three MAVs without changing the adaptation gains. The MRAC controller was tested for the uncertainty in aerodynamic coefficients by deploying the flap during flight tests. Beard *et al.* [7] used a L1 adaptive algorithm to control the pitch attitude loop for MAVs. Simulation and flight test showed that L1 adaptive controller exhibited robustness for variable sample rates, as well as for time delays. Ismail *et al.* [8] studied the roll response of MRAC and modified-MRAC adaptive control methods on an Ultra Stick UAV model. Their simulation results showed an absence of oscillations in the transient response of the roll command. Waszak *et al.* [9] used a modified nonlinear dynamic inversion technique [10] that does not require the plant model. They developed a controller for the MAV in which the control input is less than the control variables. The controller use the accelerometer measurements to adapt to the actuator failures and aircraft damage.

Kim *et al.* [11] proposed the use of neural networks for a nonlinear inverse controller that is trained off-line and a second neural network to compensate for un-modeled dynamics by training on-line using flight data. McFarland *et al.* [12] proposed a method that uses neural networks and direct adaptive control to compensate for unknown nonlinearities and un-modeled dynamics. Calise [13] used neural networks to estimate the uncertainty and to compensate for, and provide robustness to, the un-modeled dynamics of an aircraft. He demonstrated through simulation by considering the neural network-based inverse controller in a command augmentation system. Gundy-Burlet *et al.* [14] uses a neural network-based direct adaptive control in the presence of damage or failures in order to achieve desired flight control performance. Test results show that a neural flight control system can provide additional control authority under emergency conditions. Johnson *et al.* [15] devised an adaptive control method for reusable launch vehicles with control authority limitations. Neural network adaptations are used to control the system without scheduled gains and aerodynamic data. Johnson *et al.* [16] developed an adaptive controller based on a pseudo-control hedging technique and applied this to adapt for modeling errors in a six degree-of-freedom (DOF) autonomous helicopter. Flight testing results shows that the controller is able to adapt for the modeling errors in the system dynamics. Cao *et al.* [17] developed the L1 adaptive controller technique in which a companion model adaptive controller (CMAC) enables tracking and a filtering technique using a low-pass filter in the feedback loop enables guaranteed transient performance. Many excellent papers on L1-based adaptive control are available in literature [18–22]. At Wichita State University, Pesonen *et al.* [1] developed a neural network-based adaptive longitudinal flight control system and used simulation to show the controller capability to adapt for modeling errors and control surface and engine failures. Steck *et al.* [23] studied the effect of turbulence on the neural network-based adaptive controller. Using a first-order filter on the elevator command signal, simulation results showed reasonably good adaptations for the velocity and flight path angle commands.

Rajagopal *et al.* [24] proposed an observer-controller design that separates the observer and controller functions, thereby enabling the use of high adaptation gains. The modified state observer (MSO) estimation error dynamics are determined much faster than the systems dynamics. This allows for large adaptive gains without introducing the typical oscillations associated with high gain adaptation on the system error dynamics. This controller structure was tested in simulation for the short-period dynamics of a fighter aircraft and the results are compared with those obtained using the L1 adaptive control technique [24]. Pappu *et al.* [25] used the MSO-based adaptations to remove the undesired Power Lever Arm (PLA) oscillations that are observed during the flight tests of a neural network-based MRAC adaptive controller for a general aviation aircraft. The longitudinal adaptive capabilities were tested on the ground, as well as in flight, using the Beech Bonanza aircraft [26].

This paper presents the adaptive capabilities of the modified state observer-based adaptations for the Black Kite micro aerial vehicle, both in calm air and in the presence of atmospheric turbulence. Section 2 details the architecture of the adaptive controller. Section 3 gives a description of the geometric properties of the Black Kite MAV and the equations that represent the mathematical model of the aircraft. The Proportional-Integral (PI) controller and the longitudinal dynamic inverse controller design is presented in Section 4. Section 5 details the turbulence model, simulation test cases, and response plots for typical test conditions with, and without, turbulence. The development of the mathematical model of the aircraft is shown in the Appendix.

2. Modified State Observer Architecture

The MSO-based adaptive controller combines the observer feature and neural network-based basis function approximations to compute the adaptations. The dynamics of the MAV are represented by Equation (1):

$$\left[\dot{x}_T, \dot{x}_m\right] = f\left(x_T, x_m, u\right) + d\left(x_T, x_m, u\right) \tag{1}$$

The term $f\left(x_T, x_m, u\right)$ represents the known nonlinear dynamics and $d\left(x_T, x_m, u\right)$ represents the unknown dynamics of the vehicle. x_T is the vector of states that are controlled, say $[h\ V]^T$, h is the altitude and V is the aircraft's velocity. x_m is the vector of measurable states, say $[\alpha\ \overline{q}]^T$, α is the angle of attack and $\overline{q}$ is the dynamic pressure. u is the vector of control inputs and, for longitudinal dynamics, it can be $[T\ \delta_e]^T$. T is the engine thrust and δ_e is the elevator deflection. The variables $\dot{x}_T$ and $\dot{x}_m$ are the rate of change of controlled and measured states, respectively. To estimate the unknown dynamics, Equation (1) is rewritten in observer structure as in Equation (2):

$$\dot{\hat{x}}_T = f\left(x_T, x_m, u\right) + \hat{d}\left(x_T, x_m, u\right) + K_2\left(x_T - \hat{x}_T\right) \tag{2}$$

The uncertainty term $\hat{d}\left(x_T, x_m, u\right)$ is approximated as a product of the neural network-based weight vector $\hat{W}$ and basis function vector $\Phi\left(x_T, u\right)$, as $\hat{d}\left(x_T, x_m, u\right) = \hat{W}^T\Phi\left(x_T, u\right)$. The parameters of the basis function $\Phi\left(x_T, u\right)$ is the Kronecker product of the states that affect the commanded state vector x_T. The states considered are pitch angle θ, $\dot{\theta}$, and normalized velocity $V/15$. The MAV is designed to fly at the speed variations of 12 to 20 m/s. Hence, the airspeed that the MAV cruises at wing level condition (trim velocity) is set as 15 m/s. The adaptive controller performance is studied at this cruise speed. The basis function vector for the longitudinal adaptations are as in Equation (3):

$$\Phi = \begin{bmatrix} 1 & \theta\ \dot{\theta}\ \dfrac{V}{15}\ \theta\dfrac{V}{15}\ \dot{\theta}\dfrac{V}{15}\ \theta\dot{\theta}\ \theta\dot{\theta}\dfrac{V}{15} \end{bmatrix}^T \tag{3}$$

In Equation (2), K_2 is a design parameter and is a gain on the estimation error $\hat{e} = \left(x_T - \hat{x}_T\right)$ between the measured states x_T and the estimated commanded states $\hat{x}_T$. The design procedure for K_2 is described in [25]. This estimation error, rather than tracking or modeling error, is used in the Lyapunov-based stable weight update rule as given in Equation (4):

$$\dot{\hat{W}} = \Gamma\Phi\left(x_T, u\right)\hat{e}^T P - \sigma\hat{W} \tag{4}$$

Here Γ is the adaptation rate, σ is the robust term to ensure boundedness of the neural network weights, and P is the solution to the Lyapunov equation [24].

Figure 1 shows the general architecture of MSO integrated with the traditional Proportional-Integral-Derivative (PID) controller. The block "*Aircraft Dynamics*" holds the aircraft model with the un-modeled uncertainties. Under ideal conditions, the PID controller is designed to enable the aircraft to track the command. The desired command from the PID controller is fed to the inverse controller which, in turn, gives the desired inputs, say, thrust and elevator deflection to the aircraft. In the presence of uncertainties, the neural network-based approximation of the

uncertainty, $\hat{W}^T\Phi(x_T, u)$ gives the adaptations to compensate the system failures and un-modeled aircraft dynamics. Additionally, the observer structure of the MSO negates the sensor noises, if any are in the system.

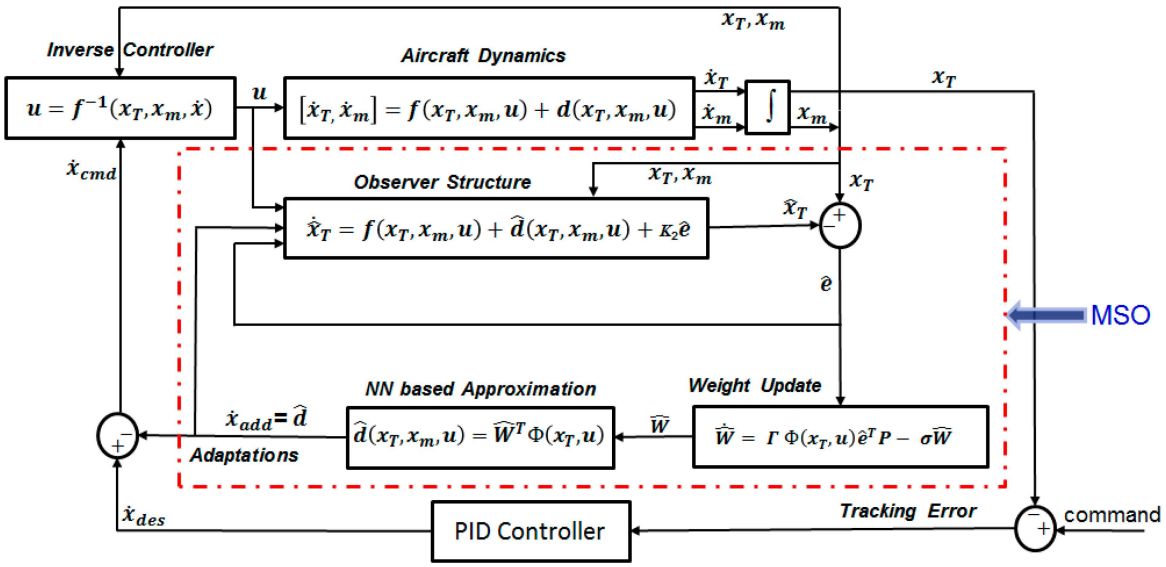

Figure 1. Block diagram of modified state observer architecture.

3. Aircraft Model

The Black Kite MAV developed by National Aerospace Laboratories (NAL) Bangalore, has an endurance of approximately 20 min, has a 2 km operational range, and flies at a cruise altitude of 60–100 m above ground level. The vehicle is designed for a cruise speed of 15 m/s and a climb rate of 2.5 m/s. The aircraft is hand-launched. It is highly maneuverable and has excellent flight characteristics. Figure 2 shows the prototype of the flying wing tractor-type Black Kite MAV.

Figure 2. Black Kite micro aerial vehicle.

The geometric properties of this aircraft are shown in Table 1.

Table 1. Geometric properties of black kite.

Serial No.	Properties		Value	Units
1	Mass, $\overline{m}$		0.29	kg
2	Wing span, b		0.30	m
3	Mean Aerodynamic Chord, c		0.25	m
4	Wing Surface Area, S		0.06118	m^2
5	Inertia	I_{xx}	0.00301326	$kg \cdot m^2$
		I_{yy}	0.00310261	$kg \cdot m^2$
		I_{zz}	0.0002636712	$kg \cdot m^2$
		I_{xz}	0.000001093	$kg \cdot m^2$
6	Moment Reference Position		(0.074,0,0)	m

An accurate mathematical model of the aircraft dynamics is developed using the nonlinear six-degree-of-freedom equations of motion. The aerodynamic and stability derivatives of the Black Kite 300 mm wing span model are obtained from wind tunnel tests conducted by NAL. Equations (5)–(13) show the linear and angular accelerations and the angular rates used to develop the aircraft model. The derivation of these equations are shown in the Appendix.

3.1. Linear Accelerations

$$\dot{u} = rv - qw - gsin\theta + X_a \tag{5}$$

$$\dot{v} = pw - ru + gsin\phi\, cos\theta + Y_a \tag{6}$$

$$\dot{w} = qu - pv + gcos\phi\, cos\theta + Z_a \tag{7}$$

where, u, v, w = body fixed linear velocity components in forward, side, and vertical directions, m/s;
$\dot{u}$, $\dot{v}$, $\dot{w}$ = linear accelerations, m/s^2;
X_a, Y_a, Z_a = body forces per unit mass, N/kg;
p, q, r = body fixed roll, pitch, and yaw rates, degree/s;
g = acceleration due to gravity, m/s^2;
θ, ϕ = Euler angles, degree.

3.2. Angular Accelerations

Solving the moment equations, the angular accelerations are as in Equations (8)–(10):

$$\dot{p} = C_3 L + C_4 N + C_2 pq + C_1 qr \tag{8}$$

$$\dot{q} = C_7 M - C_6 \left(p^2 - r^2\right) + C_5 pr \tag{9}$$

$$\dot{r} = C_4 L + C_9 N + C_8 pq - C_2 rq \tag{10}$$

where, $C_1 = \left(\left(I_{yy} - I_{zz}\right) I_{zz} - I_{xz}^2\right) / \left(I_{xx} I_{zz} - I_{xz}^2\right)$
$C_2 = \left(I_{xx} - I_{yy} + I_{zz}\right) I_{xz} / \left(I_{xx} I_{zz} - I_{xz}^2\right)$
$C_3 = I_{zz} / \left(I_{xx} I_{zz} - I_{xz}^2\right)$
$C_4 = I_{xz} / \left(I_{xx} I_{zz} - I_{xz}^2\right)$
$C_5 = \left(I_{zz} - I_{xx}\right) / I_{yy}$
$C_6 = I_{xz} / I_{yy}$
$C_7 = 1 / I_{yy}$
$C_8 = \left(I_{xx} - I_{yy}\right) I_{xx} + I_{xz}^2 / \left(I_{xx} I_{zz} - I_{xz}^2\right)$
$C_9 = I_{xx} / \left(I_{xx} I_{zz} - I_{xz}^2\right)$
$\dot{p}$, $\dot{q}$, $\dot{r}$ = roll, pitch, and yaw accelerations, $degree/s^2$;
L, M, N = roll, pitch, and yaw moments about body axis, N· m;

I_{xx}, I_{yy}, I_{zz} = moment of inertia about x, y, and z axis, kg· m^2;
I_{xz} = product moment of inertia, kg· m^2.

3.3. Angular Rates

The angular rates are related to Euler rates as in Equations (11)–(13). The Euler angles for this MAV are restricted to +/−45 degrees:

$$\dot{\theta} = qcos\ \phi - rsin\ \phi \tag{11}$$

$$\dot{\phi} = p + qsin\ \phi tan\theta + rcos\ \phi tan\theta \tag{12}$$

$$\dot{\psi} = qsin\ \phi sec\theta + rcos\ \phi sec\theta \tag{13}$$

where, θ, ϕ, ψ = Euler angles, degree;
$\dot{\theta}$, $\dot{\phi}$, $\dot{\psi}$ = Euler rates, degree.

3.4. Aerodynamic Forces and Moments

The longitudinal and lateral directional aerodynamic forces and moments are functions of the force and moment coefficients, respectively:

$$[X_a\ Y_a\ Z_a] = \frac{\overline{q}S}{\overline{m}}[C_D\ C_Y\ C_L] \tag{14}$$

$$[L\ M\ N] = \overline{q}S[bC_l\ cC_m\ bC_n] \tag{15}$$

where, C_D, C_L, C_Y = drag, lift, and side force coefficients, per radian;
C_l, C_m, C_n = roll, pitch, and yaw moment coefficients, per radian;
$\overline{q}$ = dynamic pressure, N/m^2;
S = wing planform area, m^2;
b = wing span, m;
c = chord length, m.

The MAV is equipped with elevator and aileron controls. There is no rudder. The force and moment coefficients are modeled in Equations (16)–(21).

3.5. Force Coefficients

$$C_L = C_{L0} + C_{L\alpha}\alpha + C_{L\delta_e}\delta_e + \frac{C_{Lq}qc}{2V} \tag{16}$$

$$C_D = C_{D0} + K[C_L - C_{LminD}]^2 + C_{D\delta_e}\delta_e + C_{D\delta_a}\delta_a \tag{17}$$

$$C_Y = C_{Y\beta}\beta + C_{Y\delta_a}\delta_a + \frac{\left[C_{Yp}p + C_{Yr}r\right]b}{2V} \tag{18}$$

3.6. Moment Coefficients

$$C_l = C_{l\beta}\beta + C_{l\delta_a}\delta_a + \frac{\left[C_{lp}p + C_{lr}r\right]b}{2V} \tag{19}$$

$$C_m = C_{m0} + C_{m\alpha}\alpha + C_{m\delta_e}\delta_e + \frac{C_{mq}qc}{2V} \tag{20}$$

$$C_n = C_{n\beta}\beta + C_{n\delta_a}\delta_a + \frac{\left[C_{np}p + C_{nr}r\right]b}{2V} \tag{21}$$

where, C_D, C_L, C_Y = drag, lift, and side force coefficients, per radian;

C_l, C_m, C_n = roll, pitch, and yaw moment coefficients, per radian;
δ_e, δ_a = elevator and aileron deflection, degree;
C_{Dmin} = minimum drag coefficient, per radian;
C_{LminD} = lift coefficient for minimum drag, per radian;
C_{Lq} = lift coefficient for unit change in pitch rate, per radian;
C_{D0}, C_{L0}, C_{Y0}, C_{m0} = drag, lift, side force, and pitching moment coefficients at zero-angle of attack, per radian;
$C_{D\alpha}$, $C_{L\alpha}$, $C_{m\alpha}$ = drag, lift, and pitching moment coefficients for unit change in angle of attack, per radian;
γ, α = aircraft flight path angle and angle of attack, degree;
β = side-slip angle, degree.

4. Dynamic Inverse Controller Design

The nonlinear aircraft equations of motion are dynamically inverted to design the inverse controller for the longitudinal dynamics of the aircraft. The drag, lift, and the pitching moment equations (Equations (5), (7), and (9), respectively) are modified for wings in a level flight condition $(p = r = 0)$, and the force terms X_a and Z_a are expanded to show the aerodynamic and thrust components, as shown in Equations (22)–(24). These equations are manipulated to compute the required thrust and the elevator deflection to attain the commanded linear acceleration, $\dot{V}_{cmd}$, and pitch acceleration, $\dot{q}_{cmd}$:

$$\overline{m}\left(\dot{u} + wq\right) = -\overline{m}gsin\theta + F_{A_X} + Tcos\left(\phi_T + \alpha\right) + F_{X_{\delta_e}}\delta_e \tag{22}$$

$$\overline{m}\left(\dot{w} - uq\right) = \overline{m}gcos\theta + F_{A_Z} - Tsin\left(\phi_T + \alpha\right) + F_{Z_{\delta_e}}\delta_e \tag{23}$$

$$I_{yy}\dot{q} = M_A \tag{24}$$

The pitching moment model terms of Equation (20) are measured about the hinge point of the MAV in a wind tunnel and, hence, to get an accurate rate of change of q, the moment about the center of gravity is given by:

$$M_{Tot} = \overline{q}ScC_m - F_Z\left(rAC\right) \tag{25}$$

Substituting M_{Tot} for M_A in Equation (24) and expanding C_m using Equation (20) yields:

$$\dot{q} = \frac{\left(C_{m_0} + C_{m_\alpha}\alpha + C_{m_{\delta_e}}\delta_e + C_{m_q}\left(\frac{qc}{2V}\right)\right)\overline{q}Sc}{I_{yy}} - \frac{F_Z.rAC}{I_{yy}} \tag{26}$$

where the downward force $F_Z = -\overline{q}S\left(\sin\alpha C_D + \cos\alpha C_L\right)$ and rAC is the aerodynamic center.

Substituting for force coefficients using Equations (16) and (17) for C_L and C_D and rearranging Equation (26) for elevator deflection, δ_e we get:

$$\delta_e = \frac{\left(\frac{\dot{q}_{cmd}I_{yy} + a_z rAC}{\overline{q}Sc}\right) - C_{m_0} - C_{m_\alpha}\alpha - C_{m_q}\frac{qc}{2V}}{C_{m_{\delta_e}} - \frac{b_Z.rAC}{\overline{q}Sc}} \tag{27}$$

where $a_z = -\overline{q}S\left[sin\alpha\left(C_{Dmin} + K\left(C_L - C_{LminD}\right)^2 + cos\alpha\left(C_{L_0} - C_{L_\alpha}\alpha\right) + \frac{C_{L_q}qc}{2V}\right)\right]$
$b_z = -\overline{q}S\left[sin\alpha C_{D\delta_e} + cos\alpha C_{L\delta_e}\right]$.

Combining Equations (22) and (23) to transform them to wind axis and solving for Thrust, T gives:

$$T = \frac{1}{cos\left(\phi_T + \alpha\right)}\left[\overline{m}\dot{V}_{cmd} + \overline{m}gsin\left(\theta - \alpha\right) + \overline{q}SC_{D(\delta_e=0)}\right] \tag{28}$$

where ϕ_T = thrust-line angle, positive up;
$\dot{V}_{cmd}$ = commanded acceleration, m/s^2;
T = thrust, N.

The nominal outer loop PI controller is designed based on the aircraft short-period mode characteristics. The PI gains are chosen such that they generate a closed loop rise time value close to the aircraft rise time value calculated using the short-period mode damping and frequency values. The MSO algorithm, described in Section 2, is integrated with the aircraft model along with this nominal PI controller and the dynamic inverse controller. The proportional gains for the velocity and pitch angle control loops are designed based on the required system response characteristics. The proportional and integral gain values are NAL proprietary details and, hence, are not disclosed in this paper. In normal flight conditions, the altitude, h_{cmd}, and velocity, V_{cmd}, commands are tracked by the PI controller designed for the longitudinal dynamics of the MAV. The MSO adaptations become active when the aircraft has modeling errors and failures. Figure 3 shows the integration of the PI controller and MSO adaptations with the aircraft model and dynamic inverse controller.

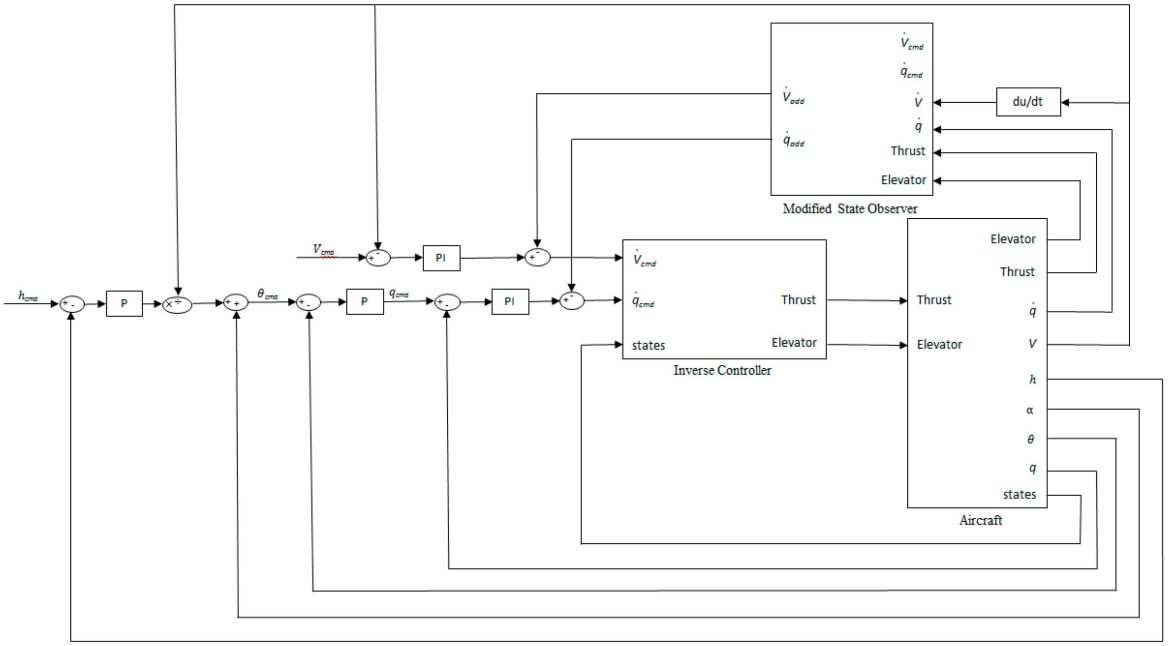

Figure 3. Block diagram of MSO adaptations and PI controller integrated with the Black Kite model and inverse controller.

5. Simulation Results

The Black Kite aircraft model integrated with MSO, PI controller, and inverse controller is modeled in MATLAB/SIMULINK® software. A Dryden turbulence model is used to model the atmospheric turbulence in the aircraft flight path. The length scale of the turbulence is set to 2 m (approximately six times the wing span length) and the turbulence intensities of 5 m/s. The International Civil Aviation Organization (ICAO) definitions of turbulence levels are given in [23], are shown in Table 2, and the load factors observed in simulation are compared with the range of load factors to interpret the results.

Table 2. International Civil Aviation Organization's (ICAO's) definitions of turbulence levels.

Level	Absolute Load Factor (n_Z) Centered around 1g	Explanation
Very Low	Below $\pm$0.05	Light oscillations
Low	$\pm$0.05 to $\pm$0.20	Choppy; slight, rapid, rhythmic bumps or cobble-stoning
Moderate	$\pm$0.20 to $\pm$0.50	Strong intermittent jolts
Severe	$\pm$0.50 to $\pm$1.50	Aircraft handling made difficult
Very Severe	Above $\pm$1.50	Increasing handling difficulty, possible structural damage

The MAV is given a ramp/step altitude command and also a step velocity command to test the capabilities of the MSO adaptations to enable the inverse controller to track the longitudinal commands in the presence of uncertainties and turbulence. Various scenarios are studied to observe the adaptation capability for the parameter uncertainties:

A. No Modeling Errors
B. Modeling Error in Aircraft
C. Modeling Error in Inverse Controller

5.1. Adaptation for No Modeling Error

The PI controller is tested in simulation to track the altitude and velocity commands with no modeling errors in the aircraft. Table 3 shows the simulation conditions and the response of the MAV with, and without, adaptations. The engine and elevator failures, if any, are activated simultaneously at 140 s. Cases 1 and 2 show the scenario in which elevator efficiency is 100% and 70%, respectively, while the engine efficiency is 100% and 25%, respectively, in the absence of turbulence. The PI controller is able to track the longitudinal commands for Cases 1 and 2. The elevator efficiency is reduced by 40% in Case 3 and the aircraft is unable to track the altitude and velocity commands both with, and without, MSO adaptations. Cases 4, 5, and 6 are similar to 1, 2, and 3, except for the introduction of turbulence. Though the PI controller is capable of tracking the commands in Cases 4 and 5, the presence of MSO adaptations reduce the effective load factor from moderate to low level turbulence. Figures 4–10 show the response of the commands, associated states, and control inputs (Elevator deflection, δ_e and Thrust, T) for Case 5.

Table 3. Simulation results—No modeling error.

Case	C_{mff}—Aircraft *	C_{mff}—Controller *	Elevator Failure, %	Engine Failure, %	Turbulence		Result			
					L, m	σ_w, m/s	Without MSO	n_Z	With MSO	n_Z
1	−1	−1	None	None	None	None	Tracks	NA	NA	NA
2	−1	−1	30	75	None	None	Tracks	NA	NA	NA
3	−1	−1	40	75	None	None	Fails	NA	Fails	NA
4	−1	−1	None	None	2	5	Tracks	Moderate 0.2 to 0.3	Tracks	Low 0.1 to 0.2
5	−1	−1	30	75	2	5	Tracks	Moderate 0.2 to 0.3	Tracks	Low 0.1 to 0.2
6	−1	−1	40	75	2	5	Fails	NA	Fails	NA

* Actual $C_{m\alpha}$ values are normalized.

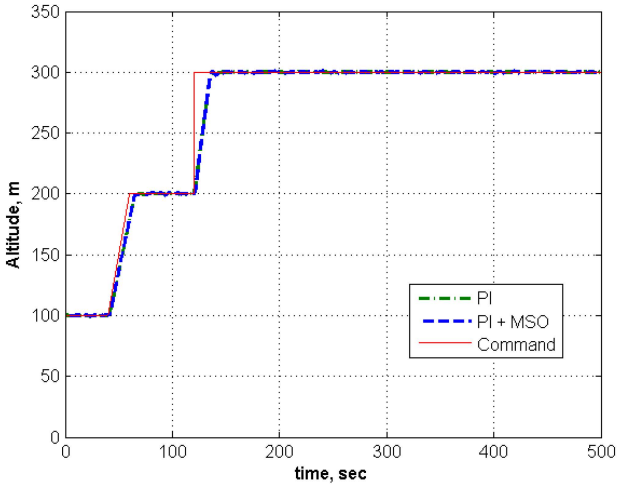

Figure 4. Altitude response for 100% $C_{m\alpha}$.

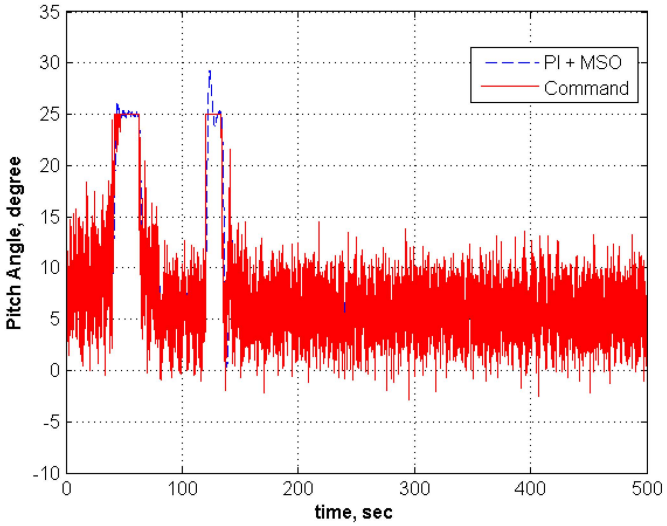

Figure 5. Pitch angle response for 100% $C_{m\alpha}$.

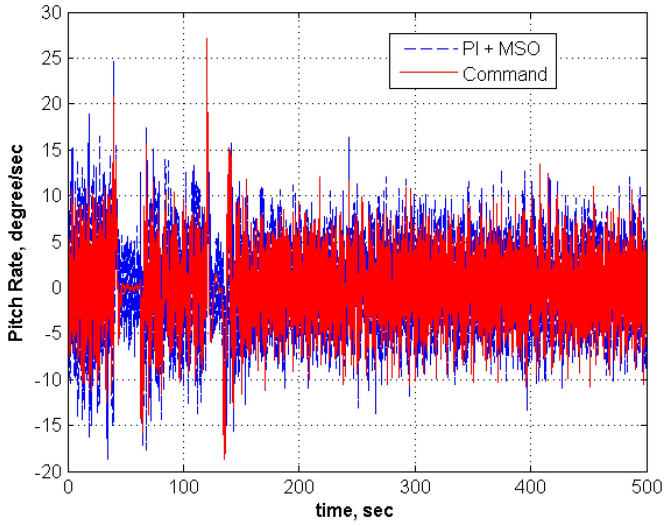

Figure 6. Pitch rate response for 100% $C_{m\alpha}$.

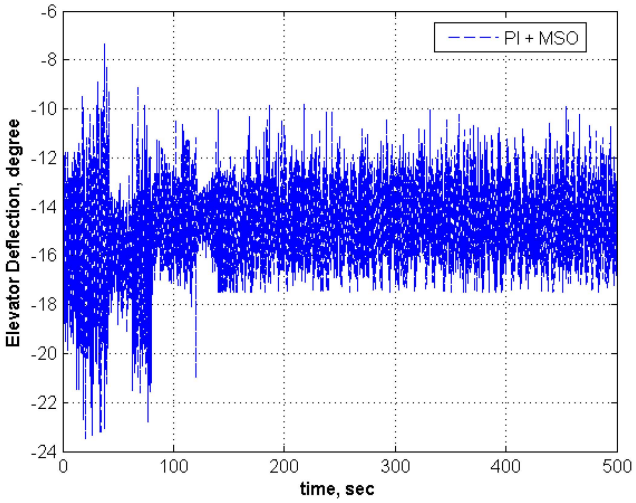

Figure 7. Elevator deflection for 100% $C_{m\alpha}$.

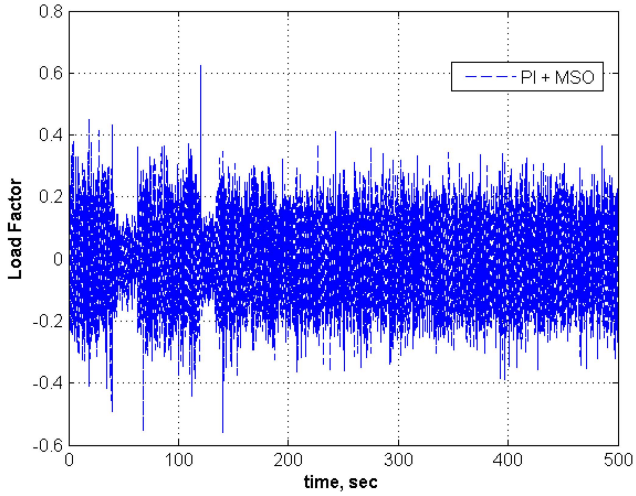

Figure 8. Load factor for 100% $C_{m\alpha}$.

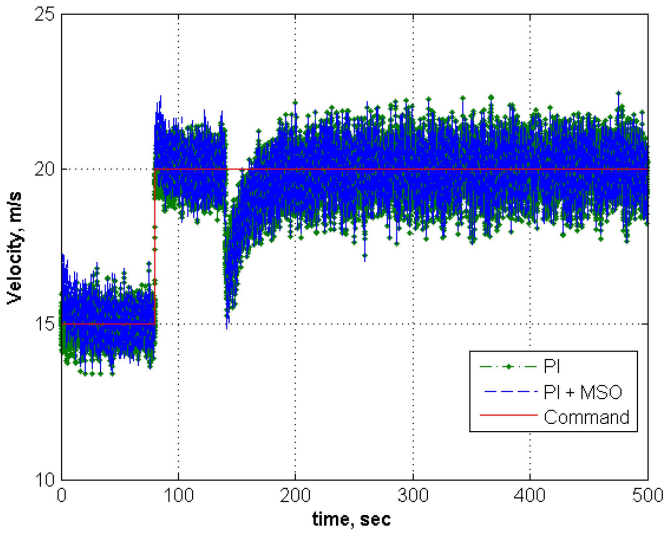

Figure 9. Velocity response for 100% $C_{m\alpha}$.

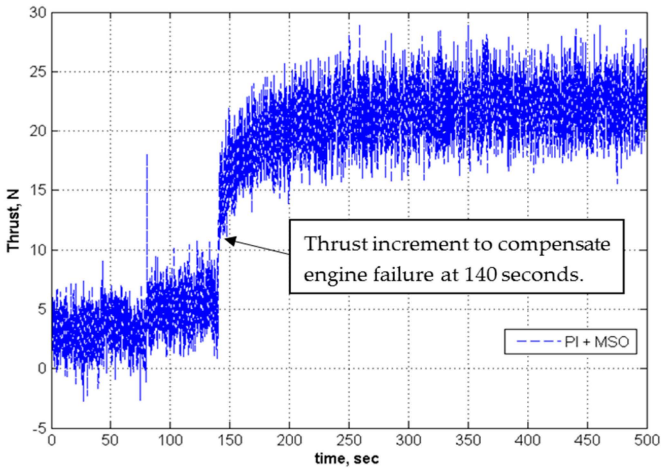

Figure 10. Commanded thrust response for 100% $C_{m\alpha}$.

5.2. Adaptation for Modeling Error in an Aircraft

The nominal PI controller, with and without MSO adaptations, is tested for the parameter uncertainties that arise from modeling inaccuracies and system failures. The aircraft pitching moment coefficient due to alpha ($C_{m\alpha}$) is reduced by 50% of the nominal design value for the aircraft ($C_{m\alpha}$ = 0.5 × design $C_{m\alpha}$). The PI controller is able to track the altitude and velocity commands in the absence of turbulence and elevator and engine failures as observed in Case 1 of Table 4. Case 2 shows the aircraft's response for reduced elevator and engine efficiency in the absence of turbulence. To simulate the critical condition, both elevator and engine failures are initiated simultaneously at 140 s. The $\dot{q}$ and $\dot{v}$ adaptations of MSO are required for the PI controller to track the h and V commands, when system failures are included in the simulation. Cases 3–5 are similar to Cases 1 and 2 with the inclusion of turbulence in simulation. The PI controller cannot track the h and V commands in the presence of turbulence, even without failures (Case 3). The MSO adaptations, along with the PI controller, enable tracking with low turbulence levels. Cases 4 and 5 shows the tracking capability of the controller along with the MSO adaptations in the presence of turbulence and failures. Low turbulence level is experienced by the aircraft for these cases. The aircraft does not have enough elevator to trim for 150% and −100% of aircraft's $C_{m\alpha}$ and, hence, Cases 6 and 7 are too much to be handled by the MSO adaptive controller. The altitude and velocity response, for Case 4, along with the states and control inputs, are shown in Figures 11–17.

Table 4. Simulation results—modeling error in an aircraft.

Case	C_{mff}—Aircraft *	C_{mff}—Controller *	Elevator Failure, %	Engine Failure, %	Turbulence		Result			
					L, m	σ_w, m/s	Without MSO	n_Z	With MSO	n_Z
1	−0.5	−1	None	None	None	None	Tracks	NA	NA	NA
2	−0.5	−1	40	75	None	None	Fails	NA	Tracks	NA
3	−0.5	−1	None	None	2	5	Fails	NA	Tracks	Low 0.1 to 0.2
4	−0.5	−1	30	75	2	5	Fails	NA	Tracks	Low 0.1 to 0.2
5	−0.5	−1	40	75	2	5	Fails	NA	Tracks	Low 0.1 to 0.2
6	−1.5	−1	None	None	None	None	Fails	NA	Fails	NA
7	1	−1	None	None	None	None	Fails	NA	Fails	NA

* Actual $C_{m\alpha}$ values are normalized.

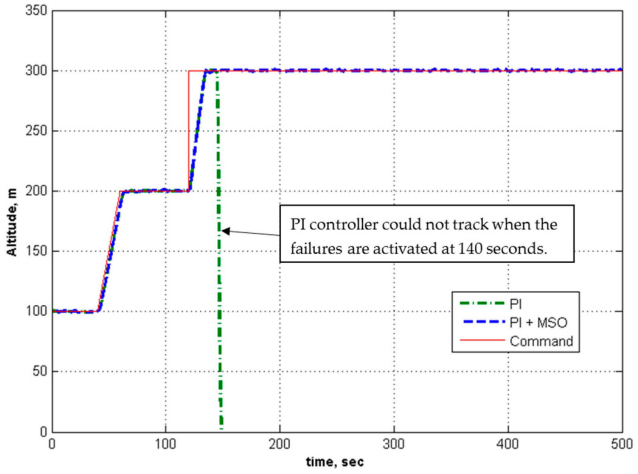

Figure 11. Altitude response for 50% $C_{m\alpha}$ in aircraft ($C_{m\alpha}$ in an aircraft = 0.5 × design $C_{m\alpha}$).

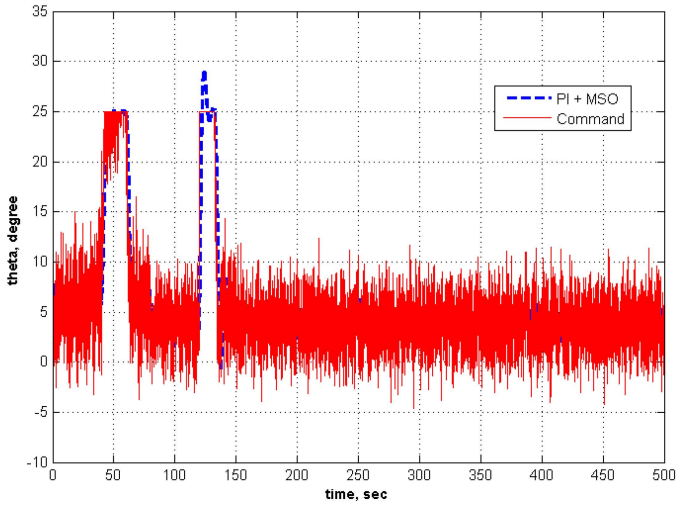

Figure 12. Pitch angle response for 50% $C_{m\alpha}$ in an aircraft.

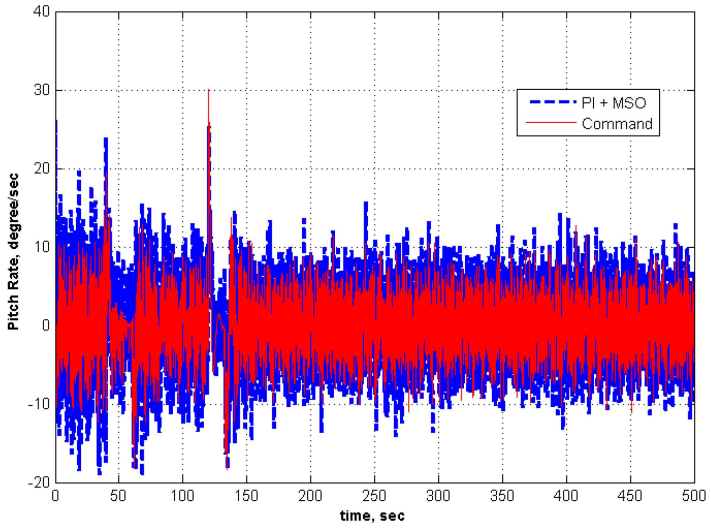

Figure 13. Pitch rate response for 50% $C_{m\alpha}$ in an aircraft.

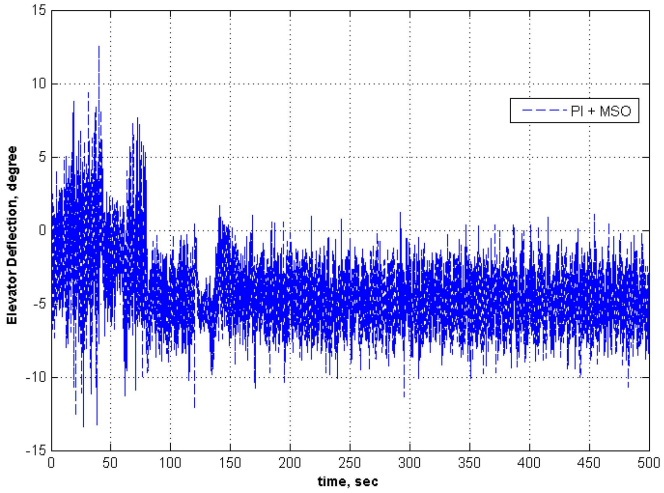

Figure 14. Elevator deflection for 50% $C_{m\alpha}$ in an aircraft.

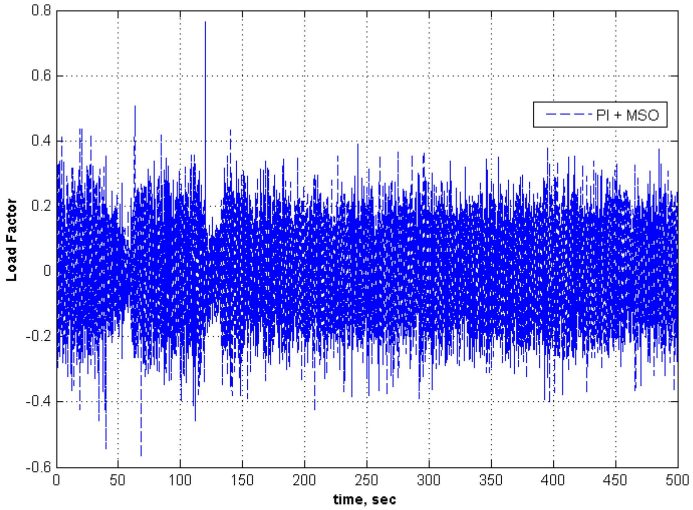

Figure 15. Load factor for 50% $C_{m\alpha}$ in an aircraft.

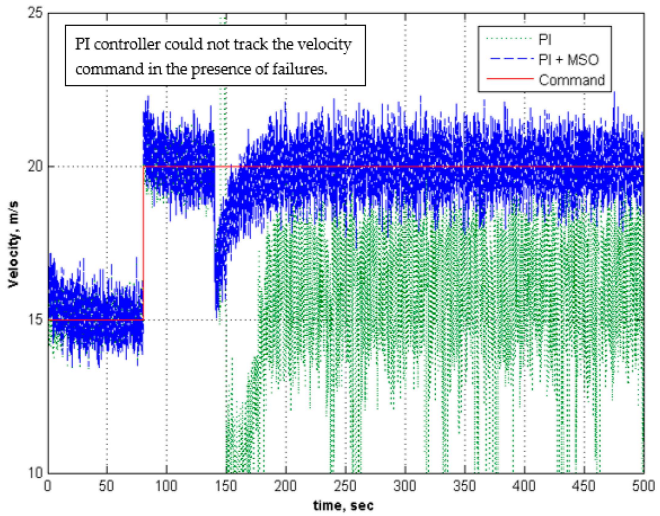

Figure 16. Velocity response for 50% $C_{m\alpha}$ in an aircraft.

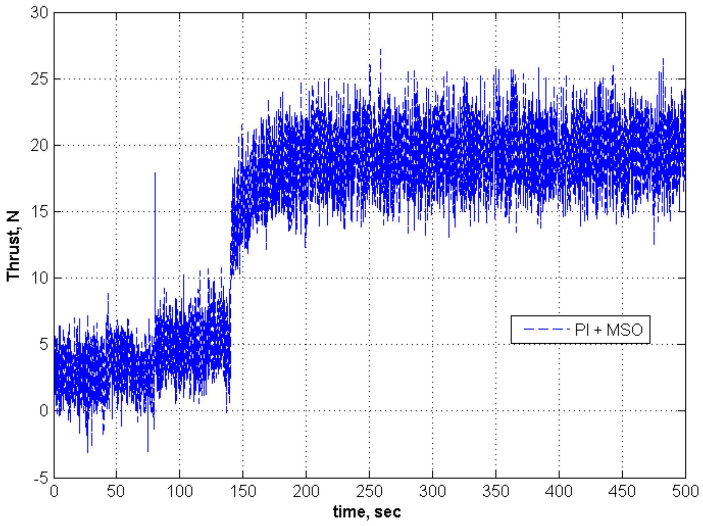

Figure 17. Thrust response for 50% $C_{m\alpha}$ in an aircraft.

5.3. Adaptation for Modeling Error in the Controller

The MSO adaptation is tested for the parameter uncertainties that arise from modeling inaccuracies in the inverse controller. The pitching moment coefficient ($C_{m\alpha}$) of the controller is varied as a percent of the nominal design value for the aircraft. The elevator and engine failures are also introduced simultaneously at 140 s in the presence of modeling errors. Table 5 shows the simulation results. Cases 1 through 6 has the controller's $C_{m\alpha}$ as 0.5 times the nominal value. Results for Case 1 and 2 shows that the PI controller is capable of tracking the altitude and velocity commands even with failures (30% elevator failure, 75% engine failure) in the absence of turbulence. So the MSO adaptations are not required for these cases. Case 3 introduces 40% elevator failure with the same engine efficiency as in Case 2. It is observed that the PI controller is not capable of tracking the commands even with MSO adaptations. Now, turbulence is introduced into the system, as seen in Cases 4–6. With the addition of MSO adaptations, the MAV experiences low turbulence levels based on the average load factor values, as noted in Cases 4 and 5. Similar to Case 3, the MSO adaptations fail to enable the PI controller to track the altitude and velocity commands as in Case 6. The aircraft's response for the controller's $C_{m\alpha}$ value of 1.5 times the nominal value is studied in Cases 7 through 10. The PI controller fails to track the longitudinal commands without MSO adaptations, as seen in Cases 7 and 8. It is observed in Case 9 that 40% elevator failure is too much for the MSO adaptations to guide the PI controller in tracking the altitude and velocity commands. Case 10 is similar to Case 7, except for the inclusion of turbulence. The MSO adaptations were not sufficient enough to equip the controller to track the commands in this case. Based on the results in Table 5, it is observed that the advantage of using the MSO adaptations, in the presence of modeling uncertainties in the controller, is limited to 30% elevator failure. Figures 18–24 show the response plots of the altitude and velocity commands for Case 5.

Table 5. Simulation results—modeling error in controller.

Case	C_{mtf}—Aircraft *	$C_{m\alpha}$—Controller *	Elevator Failure, %	Engine Failure, %	Turbulence		Result			
					L, m	σ_w, m/s	Without MSO	n_Z	With MSO	n_Z
1	−1.0	−0.5	None	None	None	None	Tracks	NA	NA	NA
2	−1.0	−0.5	30	75	None	None	Tracks	NA	NA	NA
3	−1.0	−0.5	40	75	None	None	Fails	NA	Fails	NA
4	−1.0	−0.5	None	None	2	5	Tracks	Moderate ±0.2 to ±0.5	Tracks	Low ±0.1 to ±0.2
5	−1.0	−0.5	30	75	2	5	Tracks	Moderate ±0.2 to ±0.5	Tracks	Low ±0.1 to ±0.2
6	−1.0	−0.5	40	75	2	5	Fails	NA	Fails	NA
7	−1.0	−1.5	None	None	None	None	Fails	NA	Tracks	NA
8	−1.0	−1.5	30	75	None	None	Fails	NA	Tracks	NA
9	−1.0	−1.5	40	75	None	None	Fails	NA	Fails	NA
10	−1.0	−1.5	None	None	2	5	Fails	NA	Fails	NA

* Actual $C_{m\alpha}$ values are normalized.

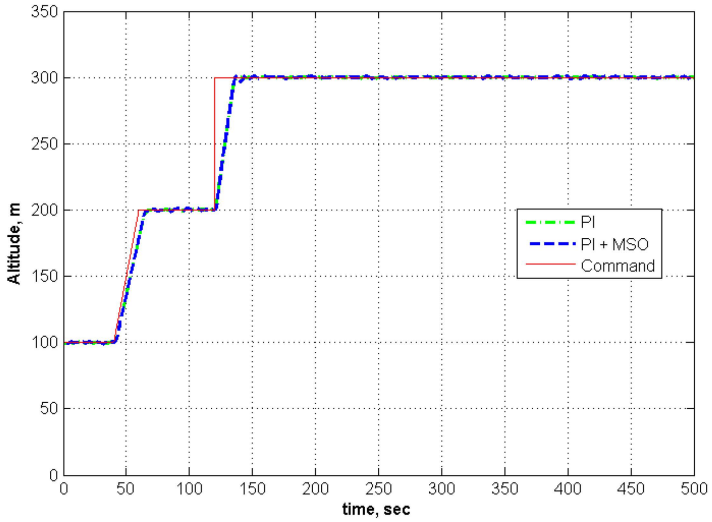

Figure 18. Altitude response for 50% $C_{m\alpha}$ in the controller ($C_{m\alpha}$ in the controller = 0.5 × design $C_{m\alpha}$).

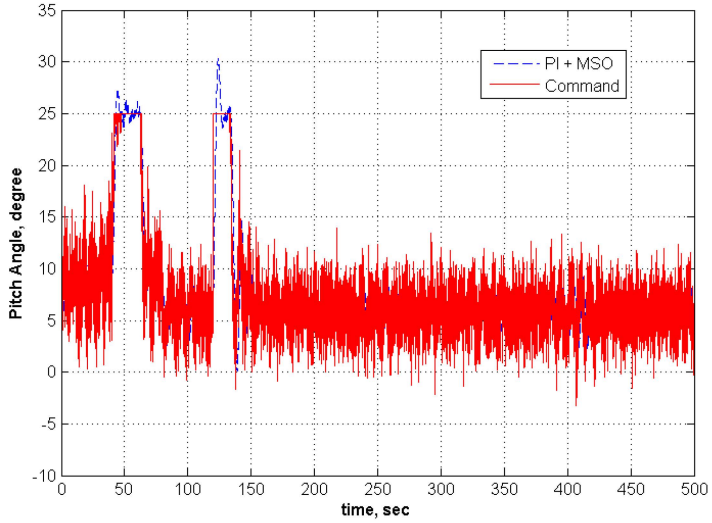

Figure 19. Pitch angle response for 50% $C_{m\alpha}$ in the controller.

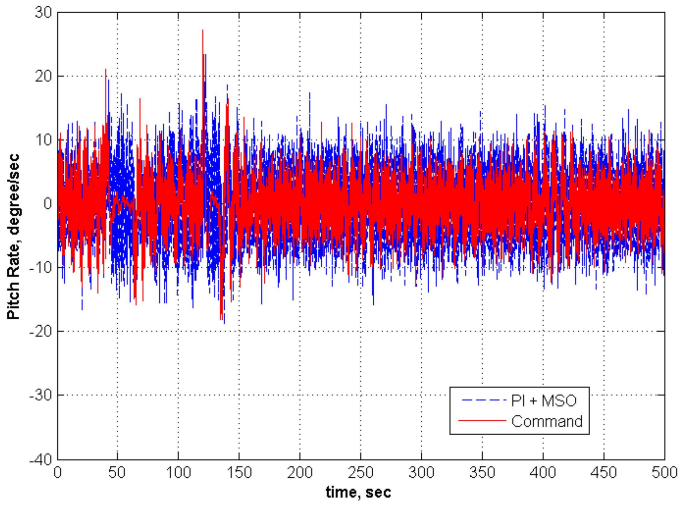

Figure 20. Pitch rate response for 50% $C_{m\alpha}$ in the controller.

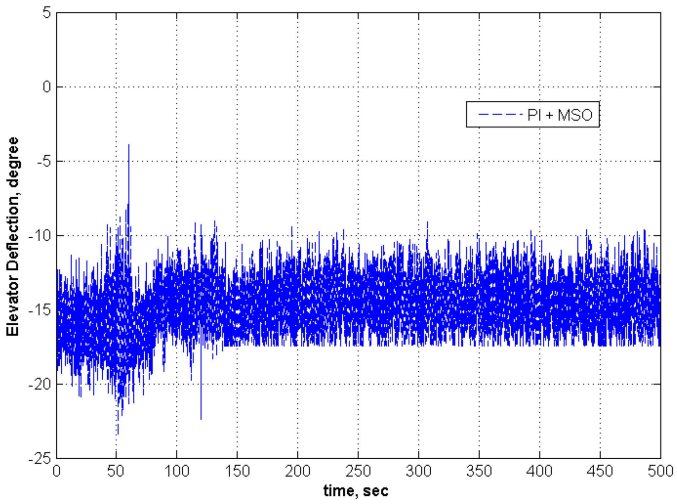

Figure 21. Elevator deflection for 50% $C_{m\alpha}$ in the controller.

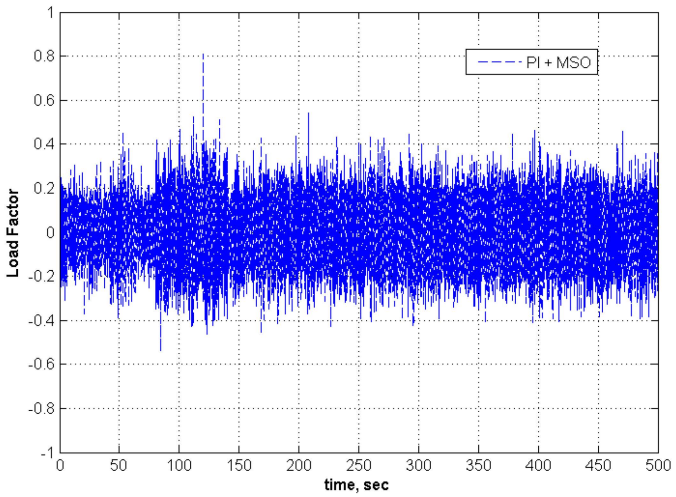

Figure 22. Load factor for 50% $C_{m\alpha}$ in the controller.

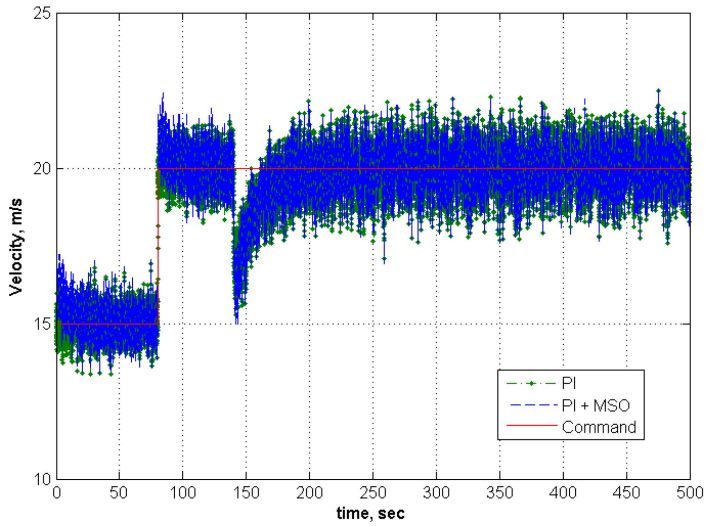

Figure 23. Velocity response for 50% $C_{m\alpha}$ in the controller.

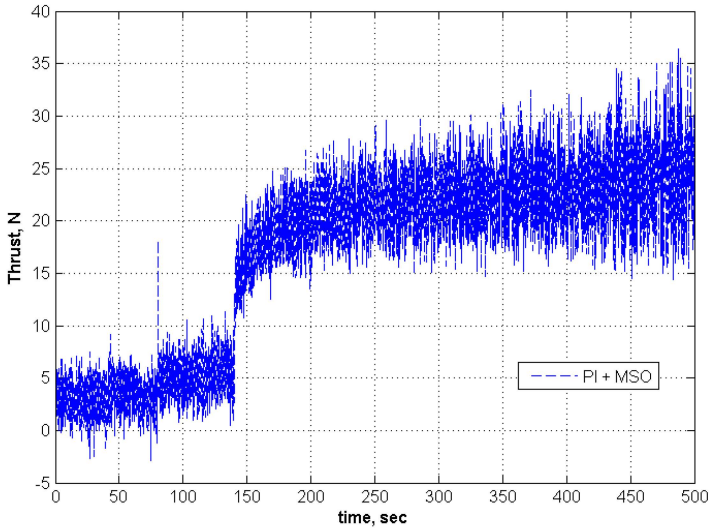

Figure 24. Thrust response for 50% $C_{m\alpha}$ in the controller.

6. Conclusions

The modified state observer-based adaptive controller is tested in simulation for its adaptive capabilities in the longitudinal dynamics of the MAV, in the presence of turbulence. The range of test cases considered shows the operational limitations of the use of MSO adaptations for the modeling error in pitching moment coefficient, and elevator and engine failures. The aircraft pitching moment coefficient is varied by $+/-$ 50%, the available elevator deflection is reduced by 40%, and the engine efficiency is reduced by 75%. The presence of MSO adaptations not only enable the PI controller to track the commands during adverse conditions, but also reduce the effect of turbulence on the MAV. This is observed from the load factor values experienced by the aircraft. The hardware-in-loop ground tests and flight tests of this adaptive controller for the longitudinal dynamics should be carried out to demonstrate its real-time adaptation capabilities.

Acknowledgments: This material is based upon the work done in NAL Bangalore, during the authors' internship program, and General Aviation Flight Lab (GAFL) at Wichita State University. The author would like to thank Shyam Chetty, Director, NAL, for his support in this research in Flight Mechanics and Control Division at NAL. Any opinions, findings, and conclusions or recommendations expressed in this material are those of the authors and do not necessarily reflect the views of the National Aerospace Laboratories.

Author Contributions: The mathematical model of the MAV using the wind tunnel data was developed by Guruganesh Ramamurthi at National Aerospace Laboratories (NAL), Bangalore, India. Venkatasubramani S. R. Pappu designed the MSO based adaptive controller for the Black Kite MAV. The PID controller design for this aircraft and overall guidance for this project was provided by Dr. James E. Steck from Wichita State University.

Conflicts of Interest: The authors declare no conflict of interest.

Appendix

Derivation of Accelerations and Angular Rates:

The force, moment, and kinematics equations of motion [27] are used to derive the linear and angular accelerations and angular rates. The force, moment, and kinematic equations in the airplane body fixed axis system are shown in Equations (29) through (37).

Force equations:

$$\overline{m}\left(\dot{u} - rv + qw\right) = -\overline{m}g.sin\theta + F_{A_X} \tag{29}$$

$$\overline{m}\left(\dot{v} - pw + ru\right) = \overline{m}g.sin\phi\ cos\theta + F_{A_Y} \tag{30}$$

$$\overline{m}\left(\dot{w} - qu + pv\right) = \overline{m}g.cos\phi\ cos\theta + F_{A_Z} \tag{31}$$

Moment equations:

$$I_{xx}\dot{p} - I_{xz}\dot{r} - I_{xz}pq + \left(I_{zz} - I_{yy}\right)rq = L \tag{32}$$

$$I_{yy}\dot{q} + \left(I_{xx} - I_{zz}\right)pr + I_{xz}\left(p^2 - r^2\right) = M \tag{33}$$

$$I_{zz}\dot{r} - I_{xz}\dot{p} + \left(I_{yy} - I_{xx}\right)pq + I_{xz}qr = N \tag{34}$$

Kinematic equations:

$$p = \dot{\phi} - \dot{\psi}sin\theta \tag{35}$$

$$q = \dot{\theta}\ cos\phi + \dot{\psi}cos\theta sin\phi \tag{36}$$

$$r = \dot{\psi}cos\theta cos\phi - \dot{\theta}\ sin\phi \tag{37}$$

Rewriting Equations (29)–(31), the linear accelerations are given as shown in Equations (38)–(40):

$$\dot{u} = rv - qw - g.sin\theta + X_a \tag{38}$$

$$\dot{v} = pw - ru + g.sin\phi\ cos\theta + Y_a \tag{39}$$

$$\dot{w} = qu - pv + g.cos\phi\ cos\theta + Z_a \tag{40}$$

For angular accelerations:

Multiply rolling moment Equation (32) by I_{zz}:

$$I_{xx}I_{zz}\dot{p} - I_{xz}I_{zz}\dot{r} - I_{xz}I_{zz}pq + \left(I_{zz} - I_{yy}\right)I_{zz}rq = LI_{zz} \tag{41}$$

Multiply yawing moment Equation (34) by I_{xz}:

$$I_{zz}I_{xz}\dot{r} - I_{xz}^2\dot{p} + \left(I_{yy} - I_{xx}\right)I_{xz}pq + I_{xz}^2qr = NI_{xz} \tag{42}$$

Summing Equations (41) and (42), and rewriting, we get the roll acceleration as in Equation (43):

$$\dot{p} = \left[\frac{I_{zz}}{I_{xx}I_{zz} - I_{xz}^2}\right] L + \left[\frac{I_{xz}}{I_{xx}I_{zz} - I_{xz}^2}\right] N + \left[\frac{\left(I_{xx} - I_{yy} + I_{zz}\right) I_{xz}}{I_{xx}I_{zz} - I_{xz}^2}\right] pq + \left[\frac{\left(I_{yy} - I_{zz}\right) I_{zz} - I_{xz}^2}{I_{xx}I_{zz} - I_{xz}^2}\right] qr \tag{43}$$

Rewriting Equation (33), the pitch acceleration is as in Equation (44):

$$\dot{q} = \frac{M}{I_{yy}} + \frac{(I_{zz} - I_{xx})}{I_{yy}} pr - \frac{I_{xz}}{I_{yy}}\left(p^2 - r^2\right) \tag{44}$$

Multiply rolling moment Equation (32) by I_{xz}:

$$I_{xx}I_{xz}\dot{p} - I_{xz}^2\dot{r} - I_{xz}^2 pq + \left(I_{zz} - I_{yy}\right) I_{xz} rq = LI_{xz} \tag{45}$$

Multiply yawing moment Equation (34) by I_{xx}:

$$I_{zz}I_{xx}\dot{r} - I_{xz}I_{xx}\dot{p} + \left(I_{yy} - I_{xx}\right) I_{xx} pq + I_{xz}I_{xx} qr = NI_{xx} \tag{46}$$

Summing Equations (45) and (46), and rewriting, we get the yaw acceleration as in Equation (47):

$$\dot{r} = \left[\frac{I_{xz}}{I_{xx}I_{zz} - I_{xz}^2}\right] L + \left[\frac{I_{xx}}{I_{xx}I_{zz} - I_{xz}^2}\right] N + \left[\frac{I_{xx}\left(I_{xx} - I_{yy}\right) + I_{xz}^2}{I_{xx}I_{zz} - I_{xz}^2}\right] pq - \left[\frac{\left(I_{xx} - I_{yy} + I_{zz}\right) I_{xz}}{I_{xx}I_{zz} - I_{xz}^2}\right] qr \tag{47}$$

For angular rates:
Multiply the kinematic Equation (36) by $sin\,\phi$:

$$qsin\phi = \dot{\theta}\, cos\phi\, sin\phi + \dot{\psi} cos\theta sin^2\phi \tag{48}$$

Multiply the kinematic Equation (37) by $cos\,\phi$:

$$rcos\,\phi = \dot{\psi} cos\theta cos^2\phi - \dot{\theta}\, sin\phi\, cos\phi \tag{49}$$

Adding Equation (48) and (49), and rearranging the terms, we get:

$$\dot{\psi} = \frac{(qsin\phi + rcos\,\phi)}{cos\theta} \tag{50}$$

Substituting $\dot{\psi}$ in Equation (35) and rearranging the terms we get:

$$\dot{\phi} = p + tan\theta\,(qsin\,\phi + rcos\,\phi) \tag{51}$$

Multiply the kinematic Equation (36) by $cos\,\phi$:

$$qcos\phi = \dot{\theta}\, cos^2\phi + \dot{\psi} cos\theta sin\phi cos\phi \tag{52}$$

Multiply the kinematic Equation (37) by $sin\,\phi$:

$$r\, sin\phi = \dot{\psi} cos\theta sin\phi cos\phi - \dot{\theta}\, sin^2\phi \tag{53}$$

Subtracting Equation (52) and (53), we get:

$$\dot{\theta} = qcos\phi - r\,sin\phi \tag{54}$$

References

1. Pesonen, U.J.; Steck, J.E.; Rokhsaz, K.; Bruner, H.S.; Duerksen, N. Adaptive Neural Network Inverse Controller for General Aviation Safety. *J. Guid. Control Dyn.* **2004**, *27*, 434–443. [CrossRef]
2. Lemon, K.A.; Steck, J.E.; Hinson, B.T.; Rokhsaz, K.; Nguyen, N.; Kimball, D. Model Reference Adaptive Fight Control Adapted for General Aviation: Controller Gain Simulation and Preliminary Flight Testing on a Bonanza Fly-by-Wire Testbed. In Proceedings of the AIAA Guidance, Navigation, and Control Conference, Toronto, ON, Canada, 2–5 August 2010.
3. Lemon, K.A.; Steck, J.E.; Hinson, B.T.; Rokhsaz, K.; Nguyen, N. Application of a Six Degree of Freedom Adaptive Controller to a General Aviation Aircraft. In Proceedings of the AIAA Guidance, Navigation, and Control Conference, Portland, OR, USA, 8–11 August 2011.
4. Arning, R.K.; Sassen, S. Flight Control of Micro Aerial Vehicles. In Proceedings of the AIAA Guidance, Navigation, and Control Conference and Exhibit, Providence, RI, USA, 16–19 August 2004.
5. Jordan, T.L.; Foster, J.V.; Bailey, R.M.; Belcastro, C.M. AirSTAR: A UAV Platform for Flight Dynamics and Control System Testing. In Proceedings of the 25th AIAA Aerodynamic Measurement Technology and Ground Testing Conference, San Francisco, CA, USA, 5–8 June 2006.
6. Knoebel, N.B.; Osborne, S.R.; Matthews, J.S.; Eldredge, A.M.; Beard, R.W. Computationally Simple Model Reference Adaptive Control for Miniature Air Vehicles. In Proceedings of the 2006 American Control Conference, Minneapolis, MN, USA, 14–16 June 2006.
7. Beard, R.W.; Knoebel, N.; Cao, C.; Hovakimyan, N.; Matthews, J. An L1 Adaptive Pitch Controller for Miniature Air Vehicles. In Proceedings of the AIAA Guidance, Navigation, and Control Conference and Exhibit, Keystone, CO, USA, 21–24 August 2006.
8. Ismail, S.; Pashilkar, A.A.; Ayyagari, R. Adaptive Control of Micro Aerial Vehicles. In Proceedings of the Symposium on Applied Aerodynamics and Design of Aerospace Vehicle (SAROD 2011), Bangalore, India, 16–18 November 2011.
9. Waszak, M.R.; Davidson, J.B.; Ifju, P.G. Simulation and Flight Control of an Aeroelastic Fixed Wing Micro Aerial Vehicle. In Proceedings of the AIAA Atmospheric Flight Mechanics Conference and Exhibit, Monterey, CA, USA, 5–8 August 2002.
10. Bacon, B.J.; Ostroff, A.J. Reconfigurable Flight Control Using Nonlinear Dynamic Inversion with a Special Accelerometer Implementation. In Proceedings of the AIAA Guidance, Navigation and Control Conference and Exhibit, Denver, CO, USA, 14–17 August 2000.
11. Kim, B.S.; Calise, A.J.; Kam, M. Nonlinear Flight Control Using Neural Networks and Feedback Linearization. In Proceedings of the Aerospce Control Systems, Westlake Village, CA, USA, 25–27 May 1993.
12. McFarland, M.B.; Calise, A.J. Robust Adaptive Control of Uncertain Nonlinear Systems Using Neural Networks. In Proceedings of the American Control Conference, Albuquerque, NM, USA, 4–6 June 1997.
13. Calise, A.J. Neural Networks in Nonlinear Aircraft Flight Control. In Proceedings of the WESCON-95, San Francisco, CA, USA, 7–9 November 1995.
14. Gundy-Burlet, K.; Krishnakumar, K.; Limes, G.; Bryant, D. Control Reallocation Strategies for Damage Adaptation in Transport Class Aircraft. In Proceedings of the AIAA Guidance, Navigation, and Control Conference and Exhibit, Austin, TX, USA, 11–14 August 2003.
15. Johnson, E.N.; Calise, A.J.; Corban, J.E. Reusable Launch Vehicle Adaptive Guidance and Control Using Neural Networks. In Proceedings of the AIAA Guidance, Navigation and Control Conference and Exhibit, Montreal, QC, Canada, 6–9 August 2001.
16. Johnson, E.N.; Kannan, S.K. Adaptive Trajectory Control for Autonomous Helicopters. *J. Guid. Control Dyn.* **2005**, *28*, 524–538. [CrossRef]
17. Cao, C.; Hovakimyan, N. Design and Analysis of a Novel L1 Adaptive Controller, Part I: Control Signal and Asymptotic Stability. In Proceedings of the American Control Conference, Minneapolis, MN, USA, 14–16 June 2006.

18. Cao, C.; Hovakimyan, N. Design and Analysis of a Novel L1 Adaptive Controller, Part II: Guaranteed Transient Performance. In Proceedings of the American Control Conference, Minneapolis, MN, USA, 14–16 June 2006.
19. Gregory, I.M.; Cao, C.; Xargay, E.; Zou, X. L1 Adaptive Control Design for NASA AirSTAR Flight Test Vehicle. In Proceedings of the AIAA Guidance, Navigation and Control Conference, Chicago, IL, USA, 10–13 August 2009.
20. Gregory, I.M.; Xargay, E.; Cao, C.; Hovakimyan, N. Flight Test of an L1 Adaptive Controller on the NASA AirSTAR Flight Test Vehicle. In Proceedings of the AIAA Guidance, Navigation and Control Conference, Toronto, ON, Canada, 2–5 August 2010.
21. Kaminer, I.; Pascoal, A.; Xargay, E.; Hovakimyan, N.; Cao, C.; Dobrokhodov, V. Path Following for Unmanned Aerial Vehicles Using L1 Adaptive Augmentation of Commercial Autopilots. *J. Guid. Control Dyn.* **2010**, *33*, 550–564. [CrossRef]
22. Wang, X.; Hovakimyan, N. L1 Adaptive Controller for Nonlinear Reference Systems. In Proceedings of the American Control Conference, San Francisco, CA, USA, 29 June–1 July 2011.
23. Steck, J.E.; Rokhsaz, K.; Pesonen, U.J.; Singh, B.; Chandramohan, R. Effect of Turbulence on an Adaptive Dynamic Inverse Flight Controller. In Proceedings of the Infotech@Aerospace, Arlington, VA, USA, 26–29 September 2005.
24. Rajagopal, K.; Mannava, A.; Balakrishnan, S.; Nguyen, N.; Krishnakumar, K. Neuroadaptive Model Following Controller Design for Non-affine Non-square Aircraft System. In Proceedings of the AIAA Guidance, Navigation, and Control Conference, Chicago, IL, USA, 10–13 August 2009.
25. Pappu, V.S.; Steck, J.E.; Rajagopal, K.; Balakrishnan, S. Modified State Observer Based Adaptation of a General Aviation aircraft—Simulation and Flight Test. In Proceedings of the AIAA Giudance, Navigation and Control Conference, National Harbor, MD, USA, 13–17 January 2014.
26. Pappu, V.S.; Steck, J.E.; Steele, B.S.; Rajagopal, K.; Balakrishnan, S. Hardware-in-Loop and Flight Testing of Modified State Observer Based Adaptation for a General Aviation Aircraft. In Proceedings of the AIAA Guidance, Navigation and Control Conference, Kissimmee, FL, USA, 5–9 January 2015.
27. Roskam, J. Airplane Flight Dynamics and Automatic Flight Controls Part I. DARcorporation: Lawrence, KS, USA, 2003.